# ADAPTIVE GUIDANCE AND CONTROL
# FOR FUTURE REMOTE SENSING SYSTEMS

James W. Lowrie † and John E. Myers ††

Martin Marietta Aerospace

## Abstract

Remote sensing missions past the era of LANDSAT D require the dissemination of high quality image data to users in near real time. Martin Marietta has developed a unique approach to onboard processing which is directed at this goal. The first step of this approach was the development of an onboard cloud detection system which has flown on an aircraft flight test and will fly on the first Shuttle experimental pallet. The second step of the approach was the development of a Landmark tracker, which has also been flown on an aircraft flight test. This paper outlines the results of these two developments and summarizes the requirements of an operational guidance and control system capable of providing continuous estimation of the sensor boresight position.

## Introduction

All forecasts of advanced technology and the future space mission models have pointed to massive increases in image data return from spaceborne sensor platforms designed to provide global monitoring of agriculture, minerals, forest, and water resources. Concurrently, the user community is requesting high quality image products in a shorter amount of time. Examination of existing and near-term mission models reveals that the end to end remote sensing system is inefficient. Over 50% and closer to 80% of all data acquired by the Landsat series remains unused due to either undesirable effects such as cloud coverage or disinteresting scene content. Also, the turnaround time between data acquisition and dissemination to the user can exceed two months due to tremendous processing requirements necessary to correct imagery for distortions. This situation is intolerable to both NASA and the user community. In summary, two major limitations of existing remote sensing missions are deterministic acquisition of high quality imagery and the timely correction of imagery for distortions. This paper outlines an approach to remote sensing which will meet future mission goals by overcoming these limitiations. The approach is centered around two subsystems. The first subsystem provides real time classification of features within a scene so that onboard decisions affecting data acquisition can be made. The second subsystem incorporates a landmark tracker into a state of the art navigation system in order to continuously predict the sensor boresight position in earth fixed coordinates.

---

†James W. Lowrie is a senior engineer at Martin Marietta Aerospace, Denver Division, working in the Advanced Automation Technology area.

††John E. Myers is a Professor of Electronics Engineering Technology at Metropolitan State College, Denver, Colorado, and consultant to Martin Marietta Aerospace, Denver Division.

## Deterministic Data Acquisition

In order to solve the problem of acquiring only desirable scenes, it is necessary to define the features which are desirable or undesirable and then to develop a system which will automatically classify scenes according to their content. For remote sensing missions, it is certainly necessary to distinguish clouds from other features, but it is also desirable to separate others such as vegetation, bare earth, and water. For example, a mission dedicated to water pollution monitoring has no desire to acquire bare earth or vegetation scenes. Therefore, for this application it is necessary to discriminate between water and other classes. Table I presents a list of mission models and the types of data selection criteria they might use.

*Table I. Data Selection Criteria for Advanced Mission Models*

| Mission Model | Data Selection Criteria |
|---|---|
| Biomass Estimation | Cloud<br>Vegetation |
| Flood Detection | Cloud<br>Water |
| Forest Fire Detection | Cloud<br>Vegetation<br>Fire |
| Water Pollution Monitoring | Cloud<br>Water<br>Water/Land Interface |
| Ice Mapping | Cloud<br>Snow<br>Ice |
| General Remote Sensing<br>(Landsat) | Cloud |

The Feature Identification and Location Experiment (FILE) was first conceived in 1976 as the first segment of a truly autonomous remote sensing system (Ref. 1). The experiment, which has flown on an aircraft flight test in early 1980 and is scheduled to fly on shuttle OFT-2, is designed around the concept that generic classes of features may be separated by spectral signature using simple algorithms. It is important to note that this experiment eliminates the need for detailed ground truth information by avoiding the temptation to separate generic clusters into finer detail. The FILE algorithm utilizes the ratio of the sensor voltages in two bands centered at .65μm and .85μm. Although the observed radiance from a feature is a function of its reflectance, incident illumination, and radiance absorption of the medium through which it is viewed, the ratio of the radiance at these two wavelengths is reasonably independent of all factors except reflectance. This principle is the basis of the FILE system and is the key to avoiding the need for ground truth. Figure I shows how various feature types can be classified with the algorithm. Water and vegetation can be separated on the basis of the ratio alone. However, since the radiance ratio

for bare land is essentially the same as for clouds and snow, these features must be separated on the bases of absolute radiance.

Although the FILE experiment has been designed to classify clouds, vegetation, bare earth, and water, the technique may be extrapolated to other target types as long as the statistics of the signatures are seperable. For example, forest fire detection could be implemented using a thermal and visual band.
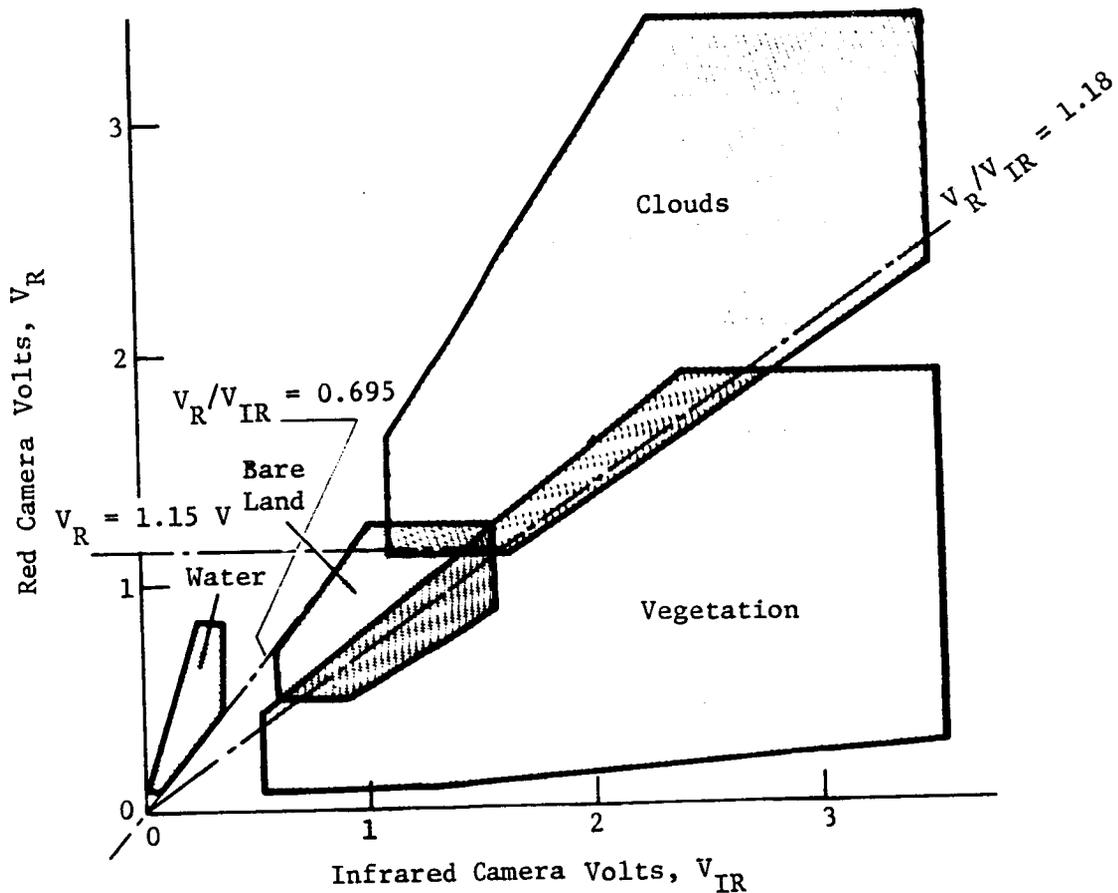


Figure I. 99% Confidence Polygons, Sun 41 to 60 Degrees from Zenth

## Image Correction

The advancement of spaceborne processors has made real time correction of imagery a feasible goal for near-term mission models provided the distortions can be measured onboard to sufficient accuracy. The primary sources of image distortion can be separated into sensor peculiarities, viewing perspective, and spacecraft characteristics (Ref. 2). With the development of linear arrays, the primary sensor-caused distortions will be the individual placement of detector elements and the orientation of the array relative to the sensor prior to flight. Viewing perspective, which is a combination of curvature of the field of view and look angle geometry, is a slowly varying function

of local earth radius and can also be considered deterministic over short intervals. The primary error source remaining, therfore, is spacecraft-caused distortions. The spacecraft error sources can be catagorized as follows:

Attitude determination

Ephemeris prediction

Misalignment between sensor and body coordinates

Mathematical inaccuracies in inertial to earth
fixed coordinate transformation

These general sources have been broken down in more detail in Table II.

*Table II.  Spacecraft Induced Error Sources in Temporal Registration*

Attitude determination
 Star tracker accuracy
 Star tracker configuration
 Knowledge of star tracker misalignment
 Error in star catalogue
 Gyro noise
 Knowledge of gyro bias, nonorthogonality, misalignment
 Numerical accuracy

Ephemeris prediction
 GPS accuracy
 Numerical accuracy

Misalignment between sensor and body coordinates
 Knowledge of linear array or scan mirror orientation
 Accuracy of thermal deflection model
 Vibration modes between two coordinates
 Calibration technique and frequency
 Numerical accuracy

Transformation error between inertial and earth fixed coordinates
 Knowledge of UT1
 Knowledge of earth precession, nutation, polar wander, and
  tidal deformation
 Numerical accuracy

    For the sake of discussion, assume that all the error is due simply to the attitude determination system. In order to achieve a temporal registration accuracy of 15 meters, it will be necessary to predict the attitude to within 4 sec as illustrated in Figure II. Accuracy of current state-of-the-art systems using the NASA standard star tracker and gyro is 15 sec ($2\sigma$) as discussed in the "Onboard Attitude Determination System" study (Ref. 3).

*Figure II. Error Budget for Registration Accuracy of 15m*

$$\phi = \tan^{-1} \frac{15m}{705km}$$

$$\simeq 4 \text{ sec}$$

705km

15m
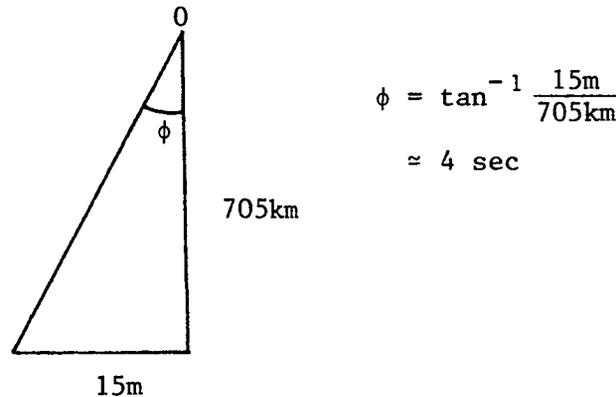
Even with the advancement of CCD star trackers, the attitude determination capability will be around 6 sec ($2\sigma$). Note that two sigma numbers have been used here corresponding to 95% of the data. If a one sigma number corresponding to 67% of the data is used, the accuracy goal can be met. However, by adding just one more error term such as a misalignment between sensor and body coordinates of 2 sec (2-axis accuracy achievable with an optical alignment cube), the total error exceeds the design goal. From the previous discussion, which ignored many error sources, it is clear that another approach is required.

Solution of the temporal registration problem requires that the sensors boresight position in earth fixed coordinates be periodically measured. This can be accomplished using a correlator which registers known Ground Control Points (GCP) within the sensor data. Onboard registration of GCPs allows many of the error terms listed in Table II to be accurately estimated in real time.

Shortly after the experimental definition of FILE, Martin Marietta began the development of a landmark tracker or GCP detector centered around our experience with terminal guidance systems. The primary function of the landmark tracker is to provide periodic measurements of the science sensors boresight position to be used as an input to a navigation system. Previous studies (Ref. 4-7) have shown that the landmark tracker will not adequately solve for both position and attitude without supplemental measurements from another source. For this reason the remote sensing navigation system has been configured with a GPS receiver to provide position measurements. Another limitation of the landmark tracker operating in the visual spectrum is that measurements are sometimes obscured by clouds and no measurements can be taken over water. For this reason, two star trackers have been added to the configuration to bound the maximum attitude error and to reduce the convergence time of the state when GCP sightings are acquired. A block diagram of the navigation system is shown in Figure III.

The registration processor is centered around a Sequential Similarity Detection Algorithm (SSDA) first identified by Barnea and Silverman (Ref. 8). Other algorithms were considered, but after significant analysis (Ref. 9), results indicate that for the advanced Landsat mission model, the SSDA is superior to other techniques due to its low probability of false lock, time required for registration, and ease of implementation in a hardwired system.
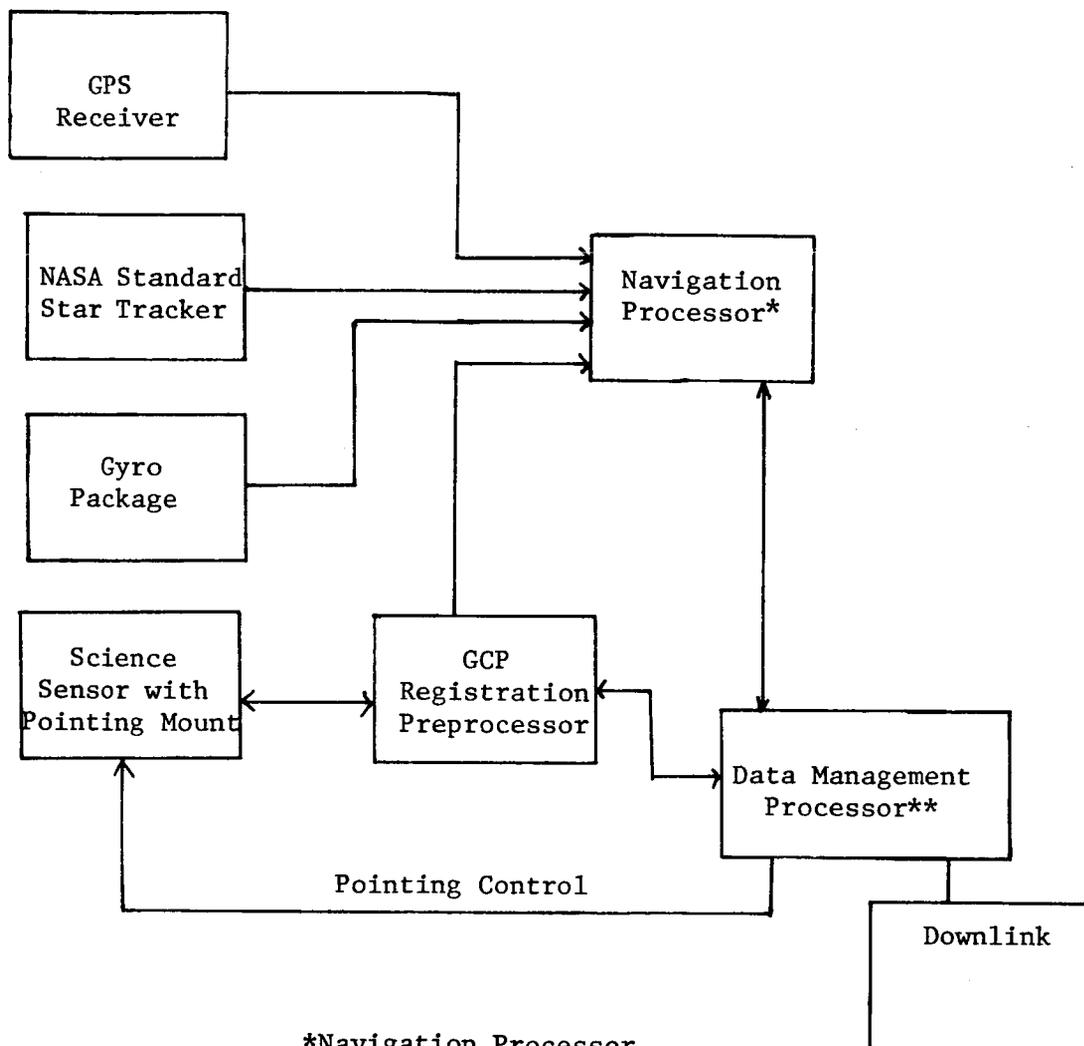
*Navigation Processor

  - Vehicle State Solution
  - Sensor Boresight
    Position Determination

**Data Management Processor

  - Data Annotation
  - Image Correction
  - Sensor Pointing
  - Information Extraction
  - Telemetry Management

*Figure III. GPS Detection System Configuration*

## GCP Registration

To perform GCP registration it is not necessary to process imagery from the entire Field of View (FOV) but only an area whose size ensures the GCP will be located within its boundary.

Let this search area be defined as an LxL area of digital picture elements. The image may be defined by a function, S, that describes the gray scale, or recorded radiance, in relation to position coordinates, i.e.,

$$S(i,j) = W_{i,j}$$

where $W_{i,j}$ is the gray scale of the $i,j^{th}$ picture element of the search area

$$1 \leq (i, j) \leq L.$$

Let the ground control point be defined similarly as an MxM area with an image function

$$G(\ell,m) = R_{1,m}$$

where $R_{1,m}$ is the gray scale of the $1,m^{th}$ picture element of the GCP

$$1 \leq (\ell, m) \leq M.$$

A subimage (Figure IV) of the SA may be defined as an MxM area whose upper left coordinates (n,o) lie in the range
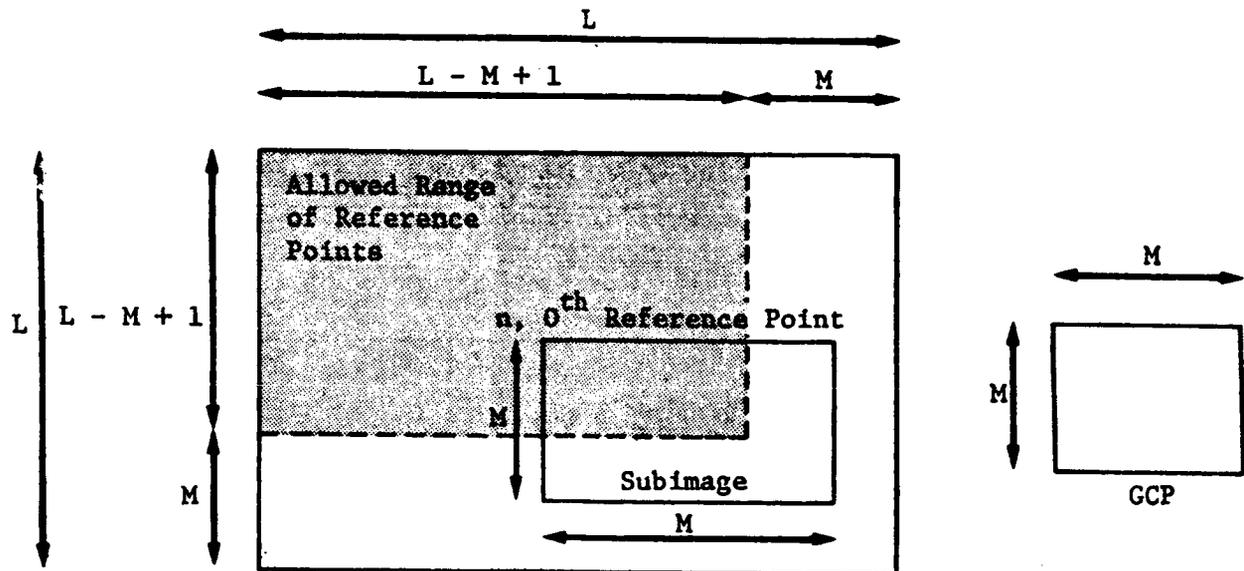
$$1 \leq (n, o) \leq L - M + 1.$$



Figure IV.  Subimage Definition

A subimage whose upper left coordinates are n,o will be referred to as the $n,o^{th}$ reference point.

The sensor data are registered by measuring the similarity between each MxM subimage within the search area and the representation of the GCP stored onboard.  The reference point that produces the highest degree of similarity with the GCP is then the best registration of the SA and can be labeled with the same earth fixed coordinates as the GCP.

The SSDA algorithm may be implemented to detect similarity between a reference point and the GCP through the following equation:

$$\text{Similarity} = \sum_{i-1}^{M} \sum_{j-1}^{M} \left| \left(S(i + n,\ j + 0) - \overline{S}_{n,o}\right) - \left(G(i,j) - \overline{G}\right) \right|$$

where

$S_{no} \equiv n,o^{th}$ reference point,

$\overline{S}_{no} \equiv$ mean value of the subimage located at the $n,o^{th}$ reference point

$\overline{G} \equiv$ mean value of the GCP.

The entire registration process can then be described by the algorithm shown in Figure V.
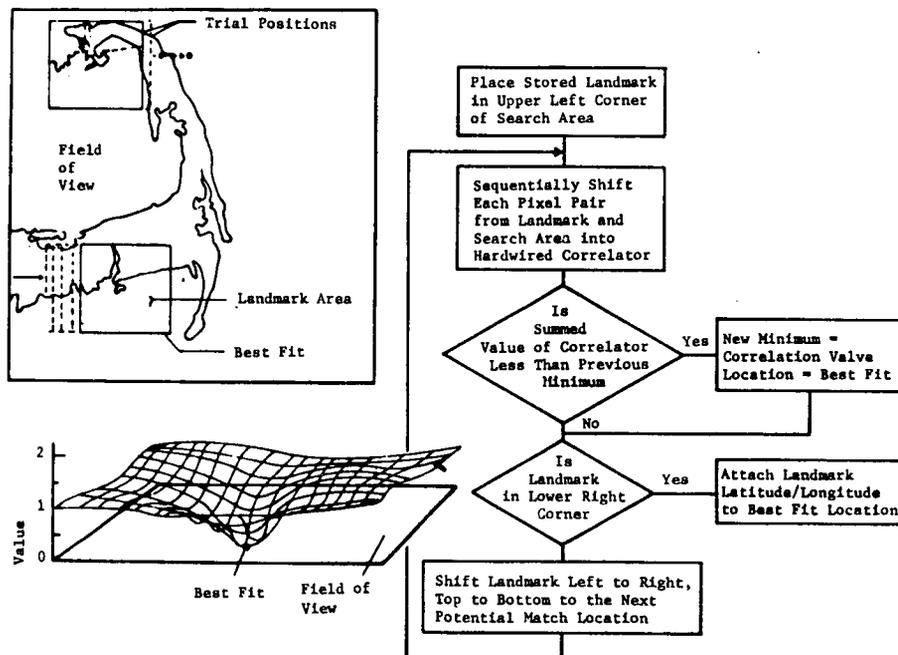


Figure V. Registration of an Area Landmark

Approaches to automatic registration have typically been limited by the effect of cloud coverage on accuracy and the inability to detect correlator false lock. A technique for reducing the effects of cloud coverage was developed under an independent research project (Ref. 9). The technique incorporates the FILE classification capability into the correlator so that every pixel representing a cloud is eliminated from the correlator computation. Results indicate that the tolerance for clouds within the search area has increased from 10% to 40%. An algorithm was also developed to detect correlation false lock. Basically, the algorithm compares the rate of convergence of the correlation surface with the rate of convergence found when the GCP is correlated with itself. If false lock is detected, no registration vector is passed to its navigation filter.

## System Model

Under contract to NASA–GSFC, Martin Marietta is currently investigating
the operational requirements of an onboard GCP detection system designed to
meet the goals of accurate image correction.  The analysis is centered around
a simulation program which models the environment of the spacecraft, generates
measurements, and estimates the state of the vehicle using an extended Carlson
square root filter.  The program was set up to provide analysis of true errors
rather than simply evaluating the covariance matrix.  Although the covariance
analysis provides a great deal of information, interpretation of results can be
inaccurate and misleading.  For example, there are many cases where the covar-
iance matrix converges over a period of time while the actual state estimate
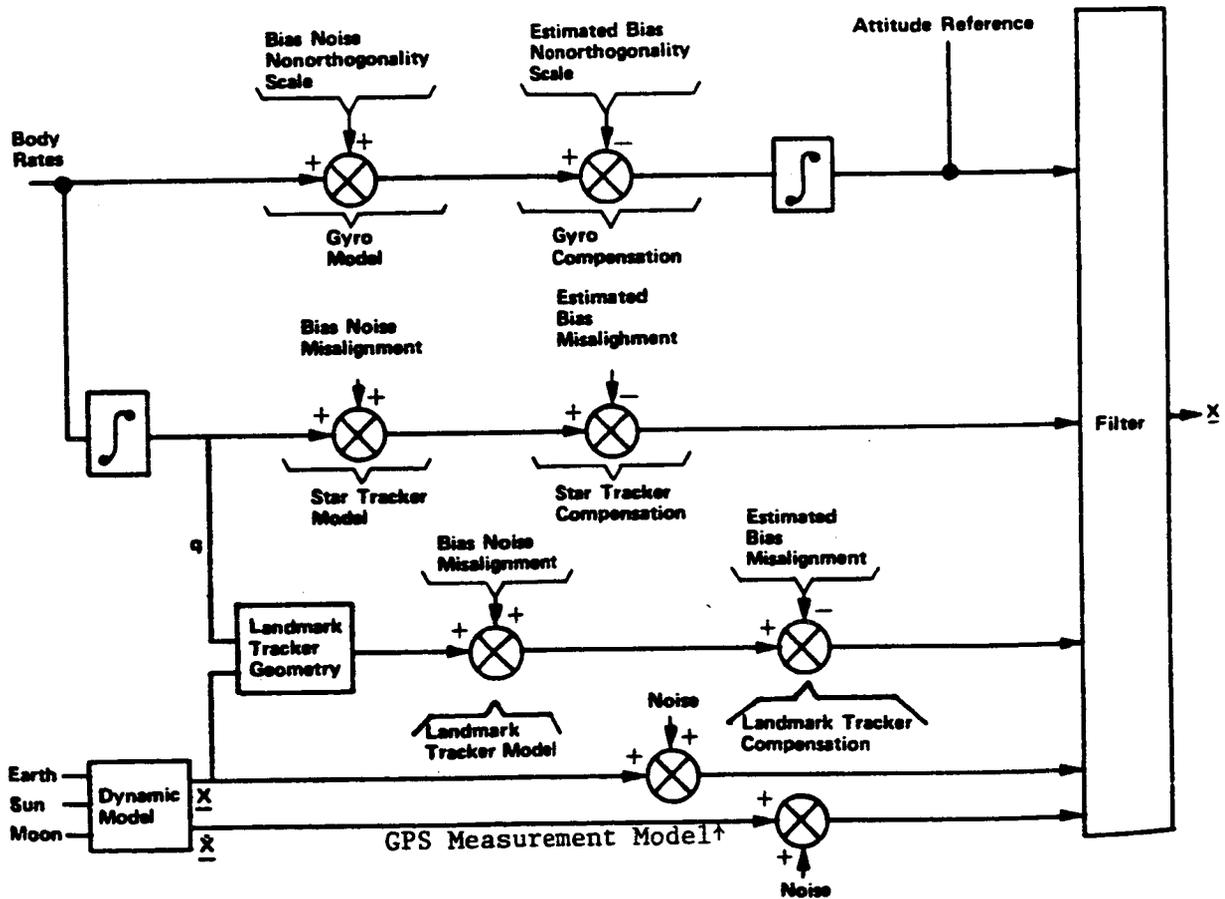diverges from the true state.  A conceptual diagram of the modeling is shown
in Figure VI.



*Figure VI.  Overview of Measurement Models*

The design philosophy behind the measurement models is that the actual
vehicle state is used with a geometry model to yield an ideal measurement
vector.  This ideal vector is then corrupted with bias, noise, and misalignment
to provide the actual sensor output.  The sensor output is then compensated for
some estimate of the error terms and is used by the filter to estimate the
vehicle state.  The benefit behind this design approach is that it enables a

detailed analysis of sensitivity to misalignments and compensation ability. It is also expected that the severe requirements associated with onboard image correction will require the onboard estimate of misalignment terms such as those between the science sensor and body coordinates. With this approach, it will not be difficult to modify the filter to solve for these terms. It is possible to understand the mathematics of most of the measurement models simply by interpreting Figure VI. However, the landmark tracker model is somewhat more complex and is described more fully here.

The landmark location on the surface of the earth in Local Landmark Coordinates (Figure VII) will be a function of the altitude ($A_L$) above the earth's mean radius.

$$\underline{L}_L = \begin{bmatrix} A_L \\ 0 \\ 0 \end{bmatrix}$$

However, in earth fixed coordinates, the landmark will have the earth's mean radius ($\overline{r}_E$) added to the altitude. Using the angular transformation from local landmark to earth fixed coordinates produces

$$\underline{L}_E = {}_E T_L \; \underline{L}_L = {}_E T_L \begin{bmatrix} \overline{r}_E + A_L \\ 0 \\ 0 \end{bmatrix} = (\overline{r}_E + A_L) \begin{bmatrix} CLC\lambda & -SL & -CLS\lambda \\ SLC\lambda & CL & -SLS\lambda \\ S\lambda & 0 & C\lambda \end{bmatrix} \begin{bmatrix} 1 \\ 0 \\ 0 \end{bmatrix}$$

$$= (\overline{r}_E + A_L) \begin{bmatrix} CLC\lambda \\ SLC\lambda \\ S\lambda \end{bmatrix}$$

As shown in Figure VII, the position vector of the spacecraft ($P_{S/C}$), when subtracted from the landmark position in some coordinate frame, will provide the measurement vector ($\underline{M}$).

$$\underline{M}_I = ({}_I T_E \; \underline{L}_E) - \underline{P}_{S/C_I}$$

Accounting for hardware misalignments, the same measurement vector in landmark tracker coordinates is:

$$\underline{M}_\ell = {}_\ell T_I \left( ({}_I T_E \; \underline{L}_E) - P_{S/C_I} \right)$$

$$= {}_\ell T_E \; \underline{L}_E - {}_\ell T_I \; \underline{P}_{S/C_I}$$

From examination of Figure VIII, the unit measurement vector in landmark tracker coordinates is:

$$\underline{U}\ell = \frac{\underline{M}\ell}{|\underline{M}\ell|} = \begin{bmatrix} U\ell x \\ U\ell y \\ U\ell z \end{bmatrix} = \begin{bmatrix} Cos\Delta VSin\Delta H \\ Sin\Delta V \\ Cos\Delta VCos\Delta H \end{bmatrix}$$

However, the tracker instrument has no sensitivity to projections along its boresight axis. Therefore, the tracker response to the unit vector $\underline{U}\ell$ will be:
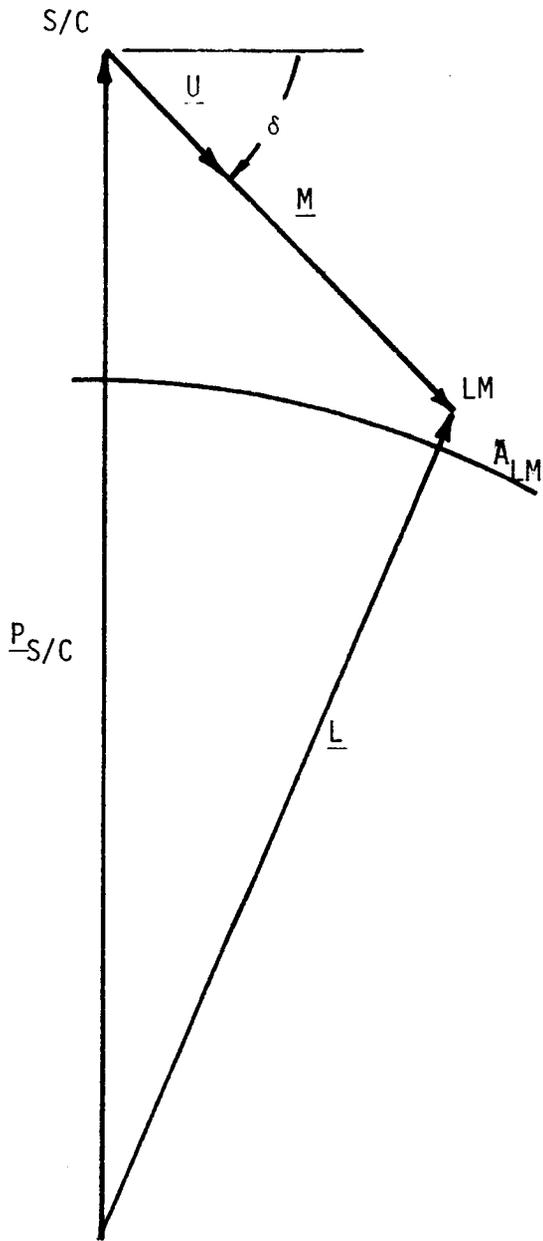
Figure VII

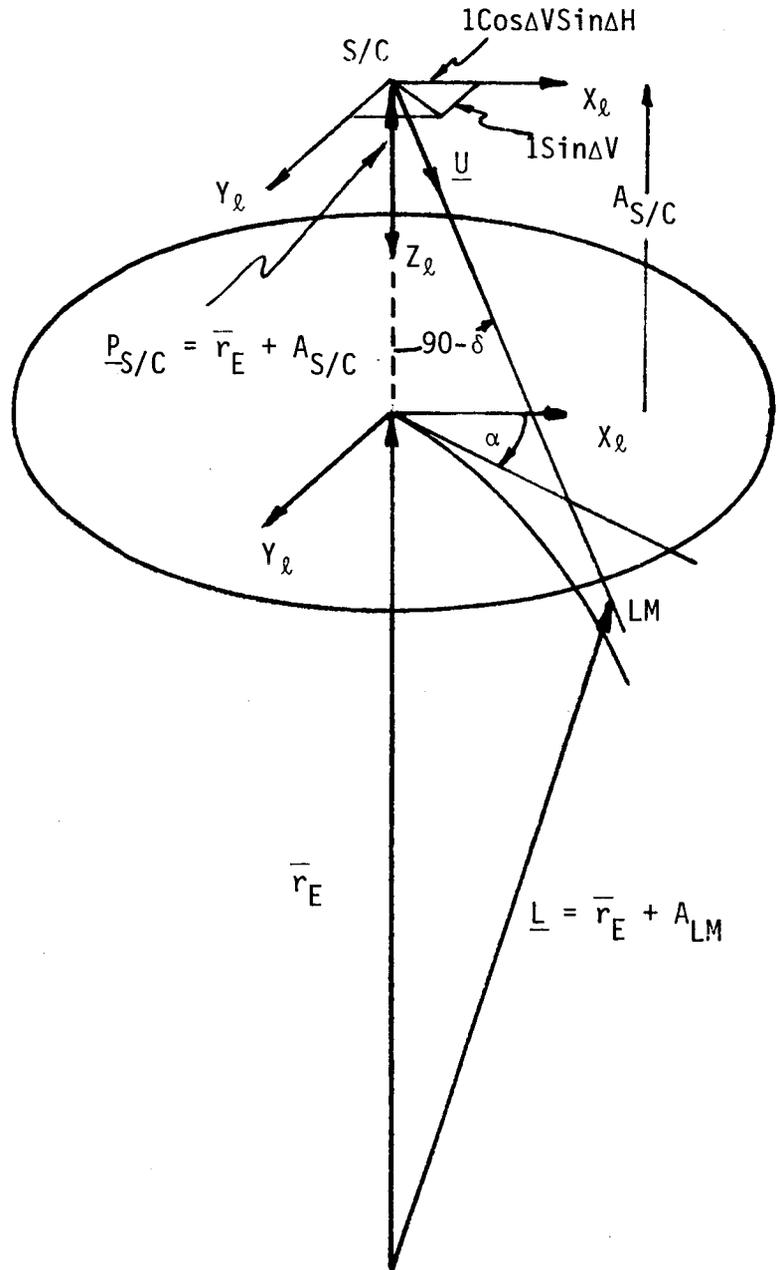Landmark Tracker Geometry –
Sighting Plan



Figure VIII

Landmark Tracker Geometry –
General

15-11

$$\underline{U\ell}' = \begin{bmatrix} U\ell x \\ U\ell y \end{bmatrix} = \begin{bmatrix} \cos\Delta V \sin\Delta H \\ \sin\Delta V \end{bmatrix}$$

producing a H and V as shown in Figure VIII as sensor outputs. Since the sensor output will be corrupted by bias and noise, the sensed measurement will be:

$$\underline{Z\ell} = \begin{bmatrix} \Delta H_s \\ \Delta V_s \end{bmatrix} = \begin{bmatrix} \Delta H + b_H + v_H \\ \Delta V + b_V + v_V \end{bmatrix}$$

Where:

$b_H$, $b_V$ = Component landmark tracker bias

$V_H$, $V_v$ = Component landmark tracker zero mean random noise, $N(0, \sigma^2)$

The component biases and standard deviations ($\sigma$) are user selectables.

The landmark tracker measurement may be compensated for knowledge of instrument bias. The bias knowledge may be a priori or through estimation. The compensated sensor output will be:

$$\underline{\hat{Z}\ell} = \begin{bmatrix} \Delta H_c \\ \Delta V_c \end{bmatrix} = \begin{bmatrix} \Delta H_s - \hat{b}_H \\ \Delta V_s - \hat{b}_V \end{bmatrix}$$

Where:

LM = the landmark being used = f (L, $\lambda$, AL)

$A_L$ = the altitude of the landmark above the mean radius of the earth

L = longitude of the landmark

$\lambda$ = latitude of the landmark

$\underline{L}$ = vector position of the landmark relative to the center of the earth

$\underline{P}_{S/C}$ = vector position of the spacecraft relative to the center of the earth

$A_{S/C}$ = altitude of the spacecraft above the mean radius of the earth

$\underline{M}$ = measurement vector from the spacecraft to the landmark

$\underline{U}$ = unit vector along $\underline{M}$

$\Delta H$ = the landmark tracker horizontal place angular deflection from the boresight axis

$\Delta V$ = the landmark tracker vertical plane angular deflection from the boresight axis

The dynamics model calculates the derivative of the spacecraft navigational state, which will be integrated to produce the navigational state vector. This is done in part by calculating the total acceleration of the spacecraft due to solar pressure and gravitation effects of the sun, moon, and earth, including fourth zonal harmonic terms. The total acceleration of the spacecraft can be

found by solving the following simultaneous equations:

$$\ddot{X}_1 = -X_1 \cdot \frac{\mu}{R^3} + g_1(t,X) + a_1(t,X)$$

$$\ddot{X}_2 = -X_2 \cdot \frac{\mu}{R^3} + g_2(t,X) + a_2(t,X)$$

$$\ddot{X}_3 = -X_3 \cdot \frac{\mu}{R^3} + g_3(t,X) + a_3(t,X)$$

where

$X = (X_1, X_2, X_3)^T$

$\mu$ = earth gravitational constant ($3.98549120E + 14 m^3/sec^2$)

$R = (X_1^2 + X_1^2 + X_1^2)^{\frac{1}{2}}$

$X_1, X_2, X_3$ = coordinates of spacecraft

$g_1, g_2, g_3$ = accelerations caused by zonal harmonics of earth gravity

$a_1, a_2, a_3$ = solar radiation pressure perturbations, sun and moon gravity

The position state is advanced in time by numerical integration of the equations of motion consisting of external forces acting on the spacecraft. Analysis of various integration algorithms has shown that the Runge Kutta Gill 4th order numerical integration method is optimal for this application. It is self-starting, handles variable step sizes, and is sufficiently accurate. The Runge Kutta Gill method for numerically integrating differential equations is described here:

The change in the value of the function during the computing interval is calculated by

$$\Delta y = \frac{1}{6} \left( k_1 + 2(1-\mu)k_2 + 2(1+\mu)k_3 + k_4 \right)$$

where

$k_1 = h \cdot f(t_n, y_n) \qquad \mu = \sqrt{2/2}$

$k_2 = h \cdot f(t_n + \frac{1}{2}h, y_n + \frac{1}{2}k )$

$k_3 = h \cdot f\left(t_n + \frac{1}{2}h, y_n + (-\frac{1}{2}+\mu)k_1 + (1 - \mu)k_2\right)$

$k_4 = h \cdot f \ t_n + h, y_n - \mu k_2 + (1 + \mu)k_3)$

$h$ = computing interval (seconds)

$t_n$ = time of beginning of computing interval (seconds)

$y_n$ = value of function at beginning of computing interval

The derivative function f is evaluated four times to calculate the change in the function being integrated during the computing interval.

Software Simulation

A Ground Control Point Simulation (GCPSIM) program has been configured to provide scientific simulations to predict the performance of the GCP detection system over a wide range of circumstances. Figure IX is a flow diagram of the
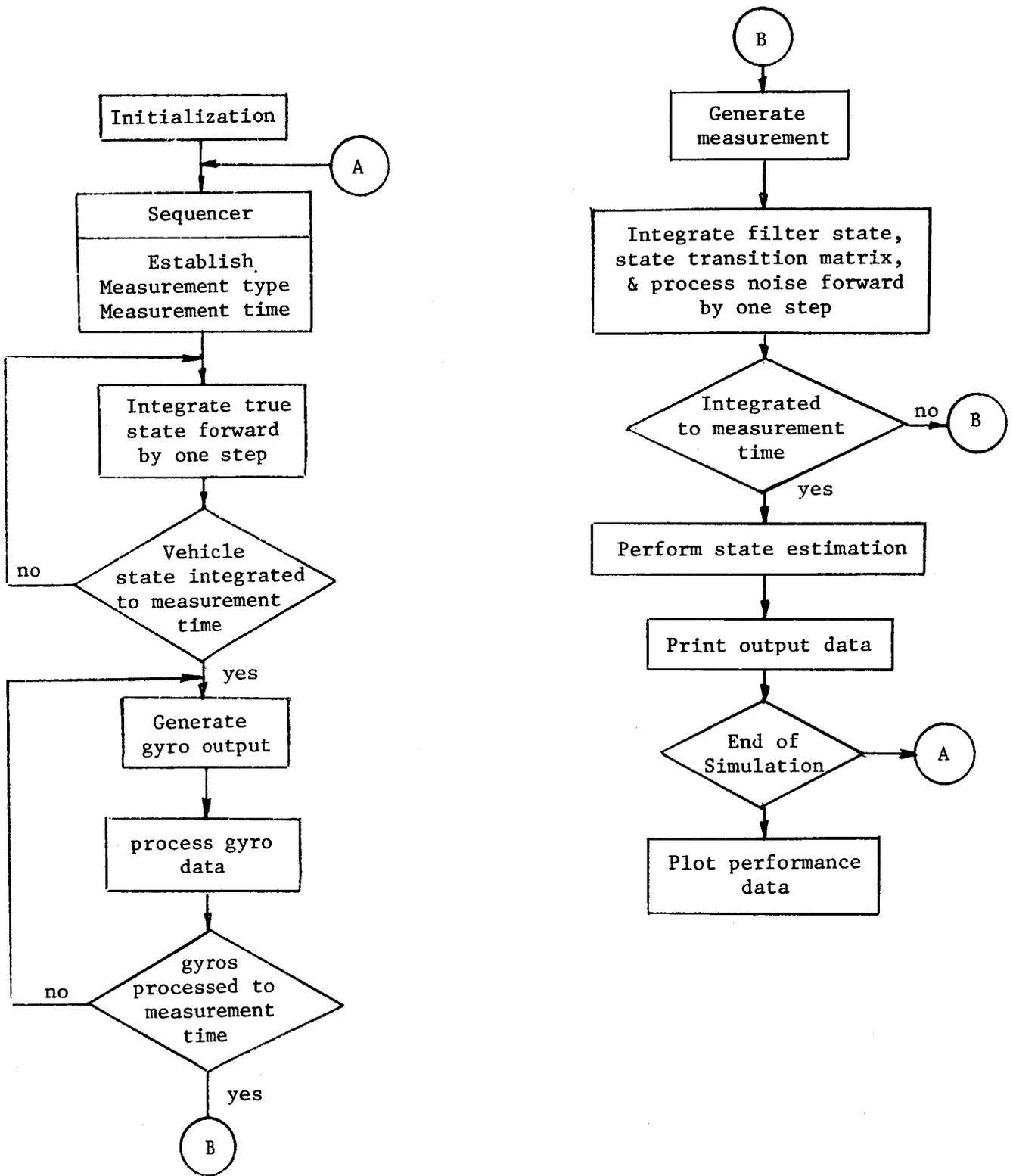
*Figure IX. Flow Diagram of GCPSIM*

simulation. GCPSIM has been designed to provide the ability to analyze the effect of various measurement sequences. This is especially important when studying the effect of GCP spacing, missed GCP sightings, and the expected accuracy after traversing a large body of water. The measurement sequencer designed for GCPSIM allows any mixture of GCP, GPS, or star tracker measurements and time delays (periods during which no measurements were made) of any length. The sequencer will determine the type of measurement and the time at which the measurement should be made. The true vehicle position state is then propagated forward to this time by integrating the nonlinear equations of motion with some additional process noise to account for modeling errors. The attitude state is propagated by looking up the body rates in an attitude profile table and integrating these rates.

The true vehicle state is used along with a measurement model to generate an ideal measurement vector. The ideal measurement is then corrupted with noise, bias, and misalignment terms and compensated for knowledge of these values. This allows a careful analysis of the effect of misalignment on the state solution. It is important to understand the effect of bias and misalignment between the landmark tracker and body axis because this is the largest unknown factor contributing to a pointing error. It is possible to calibrate the system for these misalignment errors, but it is difficult to model, for any length of time, the various processes which cause the misalignment. For example, thermal gradients across the vehicle and vibrational modes within the flexible structure are complex functions of such things as structural design, sun angle, physical properties of the material, and many other factors. These processes are the most difficult and least understood of all engineering problems. Therefore, significant emphasis will be placed on analyzing their effect on pointing accuracy.

The compensated measurements are used as inputs into an extended square root Kalman filter, which estimates the true vehicle state. The extended filter propagates the estimated navigation state, the state transition matrix, and the process noise array between measurements by integrating the various differential equations using a fourth order Runge Kutta Gill process. The estimated attitude state is propagated by a gyro model which corrupts the output with gyro drift, noise, nonorthogonality, scale factor, and misalignment. The gyro output is compensated, in a similar fasion to the measurement model, by subtracting off knowledge of these values.

The estimated state is used to form an estimated measurement which in turn is subtracted from the true measurement to obtain a residual. It is this measurement residual and a calculated Kalman gain which are used to update the state estimate. By comparing the state estimate with the true state, a direct error analysis can be performed. The entire process continues until the spacecraft is propagated forward to the run stop time.

GCPSIM has been designed to allow maximum flexibility in the analysis of an onboard landmark tracker. Types of analyses to be performed under the contract are indicated in Table III.

*Table III. Detailed Breakdown of Analysis*

| | |
|---|---|
| - Sensitivity to: | sensor accuracies |
| | sensor misalignment |
| | GCP sighting frequencies |
| | GCP location in FOV |
| | knowledge of gyro bias, noise, non-orthogonality, misalignment |
| | knowledge of earth fixed coordinates |
| | measurement sequence |
| - Accuracy given: | 1/10th pixel correlation |
| | 1 pixel correlation |
| | backup system (star tracker) |
| - Rate of Convergence: | after using backup |
| | using 1/10th pixel correlation accuracy |
| | using 1 pixel correlation accuracy |
| - Rate of Divergence: | when missing GCP sightings |
| - Ability to solve for: | sensor misalignment |
| | earth fixed coordinates |

## Summary

Development of a new generation of remote sensing systems has become a necessity for both NASA and the user community in order to fulfill the goals of future missions. In the past there has been a lack of coordination between the scientific user community and the engineers responsible for spacecraft design. This has resulted in a physical separation between the design and implementation of the science payload and the control system. This design philosophy must change if the future mission requirements are to be met.

The primary emphasis in the guidance and control system must shift from simply estimating the ephemeris and attitude of the spacecraft to estimating the position of the science sensors FOV on the earth's surface. This shift of emphasis will impact the design of the entire spacecraft. For example, if the science sensor is to be used as a primary attitude sensor, it is desirable to place the gyro package in close proximity to that sensor in order to reduce the misalignment between the two. This suggests that the current Multi-Mission Spacecraft (MMS) configuration, which provides a physical separation between the payload and the guidance and control system, will not satisfy the requirements of many future remote sensing missions.

Martin Marietta, under contract to NASA GSFC is developing an approach to remote sensing missions which eliminate the separation between the science instrument and the guidance and control system. Preliminary results obtained in the analysis of this system show great promise for automation of the end-to-end remote sensing process.

## References

1) Schappell, R. T. and Tietz, J. C., "Landmark Identification and Tracking Experiments," Remote Sensing of Earth from Space: Role of "Smart" Sensors, edited by Roger A. Breckenridge, Vol. 67 of Progress in Astronautics and Aeronautics.

2) Final Report of "On-Board Image Registration Study" prepared by TRW for NASA GSFC under Contract NAS5-23725.

3) Carney, P. C., et al, "On-Board Attitude Determination System Final Report," Martin Marietta, 1978, NAS4-23428 Mod. 27.

4) White, R. L., et al, "Use of Known Landmarks for Satellite Navigation," 1975, AIAA Paper No. 75-1097.

5) White, R. L., et al, "Attitude and Orbit Estimation Using Stars and Landmarks," 1974, IEEE Transactions on Aerospace and Electronic Systems, Vol. AES-11, No. 2.

6) Toda, N. F. and Schlee, F. H., "Autonomous Orbital Navigation by Opitcal Tracking of Unknown Landmarks," 1967, Journal of Spacecrafts and Rockets, Vol. 4, No. 12.

7) Aldrich, D. H., "Interferometer Landmark Tracker Navigation System," 1974, NEACON Journal.

8) Barnea, D. I. and Silverman, H. F., "A Class of Algorithms for Fast Digital Image Registration," IEEE Transactions on Computers, Vol. C-21, No. 2, February, 1972.

9) Lowrie, J. W. and Schappell, R. T., "Guidance and Control for an Adaptive Information Retrieval System," 1980, American Astronautical Society Paper No. AAS 80-013.